Earth, Planets and Space

FULL PAPER

Open Access

Statistical study of PMSE response to HF heating in two altitude regions

Safi Ullah[1], Hailong Li[1*], Abdur Rauf[1], Lin Meng[1], Bin Wang[1] and Maoyan Wang[2]

Abstract

Polar mesospheric summer echoes (PMSE) often show different layers. Artificial electron heating experiments are an important diagnostic tool to investigate the parameters in the PMSE regions. The response of PMSE to high frequency heating in the lower (80–85 km) and upper (85–90 km) PMSE layers is studied by analyzing PMSE observations carried out by the EISCAT VHF radar in July 2007. Different characteristics of modulated PMSE (e.g., PMSE intensity reduction, recovery, overshoot, ratios during the heating-on and heating-off times) are analyzed and compared at different situations such as only in one layer (lower or upper) and in both layers simultaneously without high-energy particle precipitation. Based on statistical results, it is found that in the lower layer all characteristics of modulated PMSE except PMSE recovery are greater than that in the upper layer. Electron temperature enhancement and PMSE modulation index due to ionospheric heating were calculated to show the enhanced electron temperature effect on PMSE. It is found that in both layers usually higher electron temperature enhancement corresponds to higher PMSE modulation index. However, the comparison of statistical results shows that in the lower layer electron temperature enhancement and PMSE modulation index are greater than that in the upper layer. Based on the relation of electron temperature enhancement to the PMSE modulation index, it is concluded that the variability of electron temperature enhancement may be responsible for the variations in different modulated PMSE characteristics between the lower and upper layers.

Keywords: PMSE, Overshoot, Active experiments, Plasma temperature and density

Introduction

At polar latitudes of earth's mesosphere, there is an intriguing observational radar phenomenon caused by the electron density irregularities due to electron charging on dust, called polar mesospheric summer echoes (PMSE) (Ecklund and Balsley 1981). PMSE has been observed by different radars having operating frequencies in the range of 50-MHz to 1.3-GHz. The growth of water ice condensation on nuclei mostly meteoric particles produces noctilucent clouds (NLC). Many investigations show the dust layers (Berger and Von Zahn 2002) and their relation with PMSE (Eremenko et al. 2005). Different dust particle sizes make the difference in the visibility of NLC and PMSE (Eremenko et al. 2005). More details of this process can be found in Rapp and Thomas (2006). NLC and PMSE are formed from submicron and nano-meter sized particles, respectively. The local plasma distribution is affected by electrons and ions attachment on dust particles (Rapp and Lübken 2003). For high dust density, a large number of electrons absorbed by the dust particles produce a local reduction in the electron density called bite-out (Havnes et al. 1996; Mitchell et al. 2001). Recently, a qualitative analysis method was presented for the analysis of dust distribution in the PMSE region (Ullah et al. 2018). Mesospheric ice particle existence is strongly supported by the occurrence of electron bite-out (Friedrich et al. 2009).

Chilson et al. (2000) observed for the first time that the PMSE strength is reduced when the mesosphere is heated with radio waves. Rapp and Lübken (2000) explained that artificial electron heating enhances the electron temperature within the dust density profile. Belova et al. (1995) showed theoretically that the electron temperature can

*Correspondence: hailong703@163.com
[1] School of Electronic Science and Engineering, University of Electronic Science and Technology of China, Chengdu, China
Full list of author information is available at the end of the article

be enhanced a few thousand degrees Kelvin due to radio waves heating. Kassa et al. (2005) showed that when the radio wave is absorbed at an altitude lower than PMSE layers, then the temperature can be enhanced more than a thousand degrees Kelvin. Normally, the strength of PMSE after the heater is switched-on and switched-off decreases and increases, respectively (Belova et al. 2003). The short switching-on and switching-off times (either 10 or 20 s) are not enough for the dust charges to relax back to their undisturbed state (Havnes 2004). During the heater-on period, the electron attachment on dust particles increases; consequently, the dust particles become more negatively charged (Kassa et al. 2005; Routledge et al. 2011). Recovery of PMSE during heating is the result of increased electron attachment on dust. After the heating is switched-off, the increased negative charges on dust increases the PMSE strength several times compared to its strength before the heater was switched-on and is known as PMSE overshoot effect (Havnes 2004). This effect is the result of an extended heating-off period. Also, some research interests are diverted toward polar mesospheric winter echoes (PMWE) because artificial electron heating has the identical effect on polar mesospheric winter echoes (Belova et al. 2008). For more details of heating effect on PMWE, see references (Havnes and Kassa 2009; Mahmoudian et al. 2016).

So far, VHF and UHF radars have been used along with EISCAT heating facility for the observations of the PMSE overshoot effect (Rietveld et al. 1993, 2016). It has since proved that the overshoot effect can be used as an effective diagnostic method (Biebricher et al. 2006). One of the noticeable unsolved issues is the charging process of dust in mesosphere. For analysis of the dust charging process, further improvement is required in the ground- and space-based experiments. For the study of dust charging process, the active ground-based heating experiments have great potential (Scales and Mahmoudian 2016). Theoretical studies include those of Biebricher et al. (2006) and Havnes et al. (2004). Also, Scales and Chen presented a series of theoretical articles (Scales 2004; Chen and Scales 2005). To use PMSE modifications through heating as a diagnostic tool, Havnes developed a theoretical model to explain the overshoot effect for VHF radar data (Havnes et al. 2003; Havnes 2004). For a range of radar frequencies and dust parameters, the original model does not perfectly predict the temporal evolution of modified PMSE because it neglects the finite diffusion time effect by using Boltzmann model for ions and electrons. The assumption of near-instantaneous diffusion of ions and electrons holds among all the diagnostic methods with models proposed earlier except for 50 MHz and less frequencies (Chen and Scales 2005; Biebricher and Havnes 2012).

In this article, we analyze and compare for the first time the response of PMSE to HF heating at two different PMSE altitudes (80–85 and 85–90 km) in the absence of high-energy particle precipitation. The main focus of the current work is to show how the PMSE is affected by artificial electron heating in the lower and upper layers. We focus on the similarities and differences of the different characteristics of modulated PMSE in the lower and upper layers which may give additional information about the PMSE formation.

Experimental details

The observations presented here were performed in July 2007 on the dates given in Table 1 with EISCAT VHF radar located at Tromsø site. A parabolic cylindrical antenna having a total aperture of 4800 m^2 was used for the transmission and reception. A detailed explanation of EISCAT VHF radar can be found in the study of Baron (1986). EISCAT radar ran the experiment of mode

Table 1 Heating cycles having PMSE with no particle precipitation in July 2007

Days	Lower layer only (case 1)	Upper layer only (case 2)	Simultaneously both layers (case 3)	
			Lower layer of case 3 (case 3a)	Upper layer of case 3 (case 3b)
July 10	–	16	4	4
July 13	–	10	67	67
July 17	1	–	–	–
July 18	24	–	–	–
July 19	36	–	–	–
Total = 5	Total = 61	Total = 26	Total = 71	Total = 71
PMSE with particle precipitation (special case)				
Days	Heating cycles in both layers			
July 12	13			

'arc-dlayer-ht.' This mode is a special version used for heating experiments, having 1.5 MW maximum peak power, 2 s time resolution and 0.3 km height resolution. It covers an altitude from 59.7 to 139.5 km with the antenna beam pointed vertically. Autocorrelation functions with 127 lags at 1.562-ms resolution were computed by using this special version of heating experiment along with the heating facility of EISCAT Tromsø radar site (Rietveld et al. 1993; Næsheim et al. 2008). In July 2007 EISCAT heating campaign, the HF transmitter was operated at frequencies 5.423 MHz and 7.953 MHz. The maximum HF transmitter power is 1 MW with 12 transmitters at nominally 85 kW each ($12 \times 85 = 1020$ kW $= 1$ MW). However, in July 2007 experiments the transmitter power was about 0.95 MW. This power multiplied by the antenna gain gives the effective radiated power (ERP). The antenna gain is independent of the transmitter frequency for the VHF radar. Depending on the combination of transmitters, heater wave frequency and antenna array, an ERP of up to 1.2 GW can be achieved (Rietveld et al. 1993; Chilson et al. 2000). The ERP in July 2007 heating campaign was 590 MW at 5.423 MHz and 1.1–1.2 GW at 7.953 MHz. The HF transmitter was operated using *X*- or *O*-modes polarization in alternating mode. The duration of each mode was 30 min.

Data analysis

In the case of PMSE, the incoherent scatter measurements with the EISCAT radars are normally analyzed in terms of apparent electron number density. However, in this study a well-documented software package, GUISDAP (Grand Unified Incoherent Scatter Design and Analysis Program), was used for the data analysis (Lehtinen and Huuskonen 1996). The term 'apparent' electron density is used to clarify the fact that the signal is not the result of real electron density rather it is due to coherent scatter of PMSE which is added to the incoherent scatter. Such derived 'apparent' electron number densities can be converted into volume reflectivities by using the well-known relation

$$\eta = \sigma \times N_e \quad (1)$$

where η is the volume reflectivity in m^{-1}, σ is half the scattering cross section of an electron and is equal to 4.99×10^{-29} m^2 and N_e is the 'apparent' electron number density in m^{-3} (Röttger and La Hoz 1990). To minimize the effect of natural background variability of the ionosphere, all the VHF radar observations from six different days were divided into 1 h duration. Each data set was converted into volume reflectivity by using Eq. (1). Each hour contained 19 heating cycles, where the duration of each cycle was 3 min (90 data points). The heater was switched-on for 20 s (10 data points) and switched-off for 160 s (80 data points).

First, the PMSE region in both the altitude ranges (80–85 km and 85–90 km) was detected by using the threshold, $\eta \geq 5 \times 10^{-18}$ m^{-1}. Second, at both the altitude ranges the average of those 'data points' was calculated which was satisfying the threshold $\eta \geq 5 \times 10^{-18}$ m^{-1}. In this study, the PMSE radar echoes for any heating cycle were considered to be present only if two consecutive data points (4 s) before the HF heater switched-on satisfy the threshold, $\eta \geq 5 \times 10^{-18}$ m^{-1}. For any heating cycle if this threshold was not satisfied, then the data of that corresponding heating cycle were removed.

Furthermore, for any heating cycle the energetic particle precipitation was considered to be present only if at 91 km the two consecutive data points (4 s) before the heater switched-on satisfy the threshold, $\eta \geq 3.99 \times 10^{-18}$ m^{-1}. According to this condition, all those heating cycles having particle precipitation were also removed. In this study, only those heating cycles were considered where there was PMSE but no particle precipitation.

For each 1-hour data set after removing the two types of heating cycles (having precipitation and the one having no PMSE), the parameters R_0, R_1, R_2 and R_3 (as shown in Fig. 1) were calculated for the remaining heating cycles to analyze the variations in the overshoot characteristic curve (OCC) in the lower and upper layers. Each of these parameters comes from 2 s of data corresponding to different positions in OCC. For example, R_0 corresponds to PMSE intensity just before the heater is switched-on, R_1 just after the heater has been switched-on, R_2 just before the heater is switched-off, and R_3 corresponds to PMSE intensity just after the heater has been switched-off again.

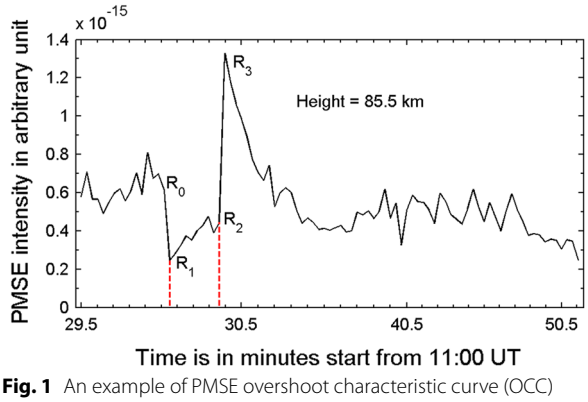

Fig. 1 An example of PMSE overshoot characteristic curve (OCC) for VHF radar on July 13, 2007, showing the backscatter sampling intervals R_0, R_1, R_2 and R_3. The heater was switched-on at 11 h 30 min UT and switched-off at 11 h 30 min 20 s UT. The heater-on time is shown between the vertical dashed lines

Results

Significant information can be obtained on the PMSE dusty plasma state by analyzing the shape of OCC during an overshoot heating cycle. A typical form of an observed OCC for a heating cycle of 20 s on and 160 s off is shown in Fig. 1. As the heating starts at 11:30 UT, the PMSE intensity immediately decreases to well below that of unaffected intensity level, followed by some recovery during the 20 s heater-on period. When the heating stops at 11:30:20 UT, then the PMSE intensity increases abruptly above the unaffected intensity level. For the rest of time, the PMSE intensity then gradually recovers to the equilibrium state (unaffected state, before 11:30 UT). Figure 2 shows an example of clear PMSE layers and heating effect. One PMSE layer from 81 to 85 km and second one from 85 to 88 km are obvious. In some heating cycles, the disappearance of PMSE when the heater is switched-on shows clear PMSE modulation. However, in other cycles the distinction of PMSE modulation is not so obvious.

The overshoot characteristic curve will change because of the different physical conditions of the PMSE within the different radar sampling volumes (Havnes et al. 2006). This should show a way that the PMSE dusty plasma conditions can be diagnosed by using PMSE overshoot as predicted and modeled earlier (Havnes 2004; Havnes et al. 2004). The ratios of different PMSE parameters (R_0, R_1, R_2 and R_3) give different PMSE characteristics. In this section, we analyze the different characteristics of PMSE in the lower and upper layers. The quantitative comparison of the strength of different PMSE characteristics between lower and upper layers is beyond the scope of this paper. This study only analyses the different PMSE characteristics macroscopically (in the case of percentage) in order to show that whether there are significant differences between how the PMSE reacts to the HF heater in the two height regions.

We analyzed the whole EISCAT heating campaign in July 2007. Table 1 shows the selected heating cycles having PMSE for different cases in July 2007. Cases 1 and 2 correspond to the heating cycles when PMSE were present only in the lower and upper layers, respectively. Case 3 corresponds to the heating cycles when PMSE were present simultaneously in both layers. In case 3, there are 71 heating cycles where PMSE occur in the lower layer (case 3a), and also occur for the corresponding time in the upper layer (case 3b). Therefore, the result of case 3 is shown in two parts. Figures 5 and 9 show the result of case 3a, and Figs. 6 and 10 show the result of case 3b.

Reduction in PMSE intensity ($R_1 < R_0$)

The first panel of Figs. 3, 4, 5 and 6 shows the ratio of PMSE intensity just after the heater switched-on to PMSE intensity just before the heater was switched-on (R_1/R_0). It is clear from Figs. 3, 4, 5 and 6 that for most of the heating cycles, the immediate reaction of PMSE to the heater being switched-on shows the decrease in PMSE intensity ($R_1 < R_0$). From Figs. 3, 4, 5 and 6, it is clear that there are greater percentage (100%) of heating cycles where $R_1 < R_0$ for case 1 as compared to all other cases.

PMSE recovery ($R_2 > R_0$)

Panel 2 in Figs. 3, 4, 5 and 6 shows the ratio of PMSE intensity just before the heater switched-off to PMSE intensity just before the heater was switched-on (R_2/R_0). The ratio $R_2 > R_0$ is defined as PMSE recovery (Havnes

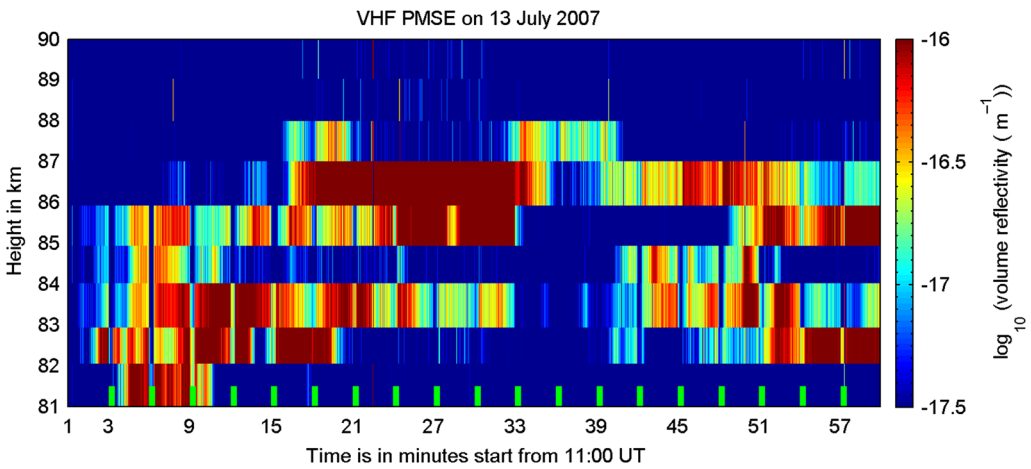

Fig. 2 An example of heater induced PMSE modulation and layers on July 13, 2007, observed by the EISCAT VHF radar. The heater-on time is shown by the green rectangles at the bottom. The HF transmitter was operated with *X*-mode for the first 30 min (11:00–11:30 UT) and with *O*-mode for the last 30 min (11:30–12:00 UT). At both modes, the frequency of transmitter was 5.423 MHz

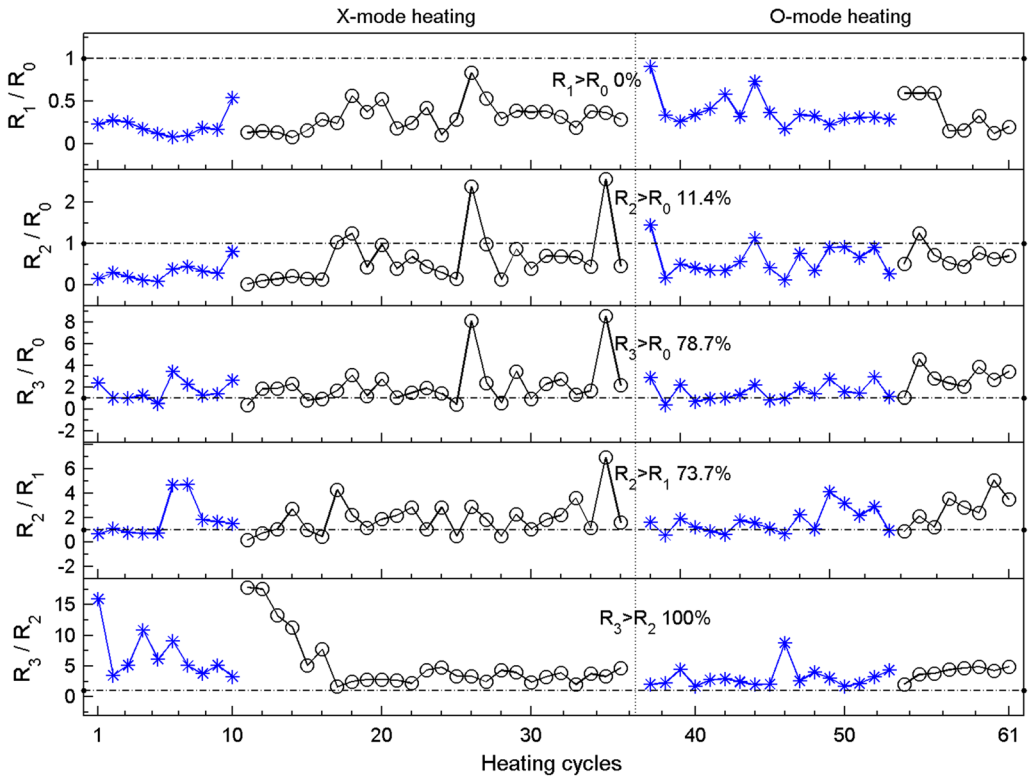

Fig. 3 The distributions of ratios of different parameters R_0, R_1, R_2 and R_3 for case 1 of Table 1. In each panel, the horizontal dashed-dotted line indicates when the ratio is equal to 1. The asterisks represent the measurements at transmitter frequency 5.423 MHz, whereas the circles represent the measurements at 7.953 MHz. The vertical dash line is used to separate the measurements of *X*- and *O*-modes polarization

et al. 2015). In panel 1 of Figs. 3, 4, 5 and 6, it is seen that most of the heating cycles first show decrease in PMSE intensity; however, for all cases in panel 2 there are some cycles which show clear PMSE recovery ($R_2 > R_0$). It is clear from Figs. 3, 4, 5 and 6 that case 2 shows greater percentage (34.6%) of heating cycles having PMSE recovery as compared to all other cases. On the other hand, panel 2 in all cases also indicates that in most of the heating cycles, the recovery ($R_2 > R_0$) is very low or completely not present therefore in all those cycles $R_2 < R_0$.

PMSE overshoot ($R_3 > R_0$)

Panel 3 in Figs. 3, 4, 5 and 6 shows the ratio of PMSE intensity just after the heater has been switched-off to PMSE intensity just before the heater was switched-on (R_3/R_0). Normally, the PMSE overshoot is defined as $R_3 > R_0$ (Havnes et al. 2015). It is clear from Figs. 3, 4, 5 and 6 that there are sufficient numbers of cycles having PMSE overshoot ($R_3 > R_0$). It is also clear from Figs. 3, 4, 5 and 6 that for case 1 there are 78.7% of cycles having PMSE overshoot ($R_3 > R_0$) which is marginally greater than case 2 (77%), and greater than cases 3a (43.6%) and 3b (62%). On the other hand, in case 3a (Fig. 5) there is a significant number of heating cycles where overshoot is not present. Such heating cycles clearly show $R_3 < R_0$.

Ratio of PMSE intensity during the heater-on time ($R_2 > R_1$)

Panel 4 in Figs. 3, 4, 5 and 6 shows the ratio of PMSE intensity during the heater-on period (R_2/R_1). It is obvious that in all cases, significant numbers of heating cycles show $R_2 > R_1$. On the other hand, in all cases there are few cycles which clearly show $R_2 < R_1$. Comparing panel 4 in Figs. 3, 4, 5 and 6, it is clear that in case 1 a greater number of cycles (73.7%) show $R_2 > R_1$ as compared to cases 2 (69.2%), 3a (45%) and 3b (67.6%).

Ratio of PMSE intensity at the heating-off time ($R_3 > R_2$)

Panel 5 in Figs. 3, 4, 5 and 6 shows that in all cases at the heating-off time, the PMSE intensity rapidly increases so that $R_3 > R_2$. For cases 1 and 2, the increase in PMSE intensity ($R_3 > R_2$) dominates. $R_3/R_2 > 1$ for 100% of heating cycles in case 1 and for 96.1% of heating cycles in case 2. From Figs. 5 and 6, it is clear that in cases 3a and 3b there are 93% of heating cycles where $R_3 > R_2$. In all cases, no heating cycle clearly shows $R_3 < R_2$.

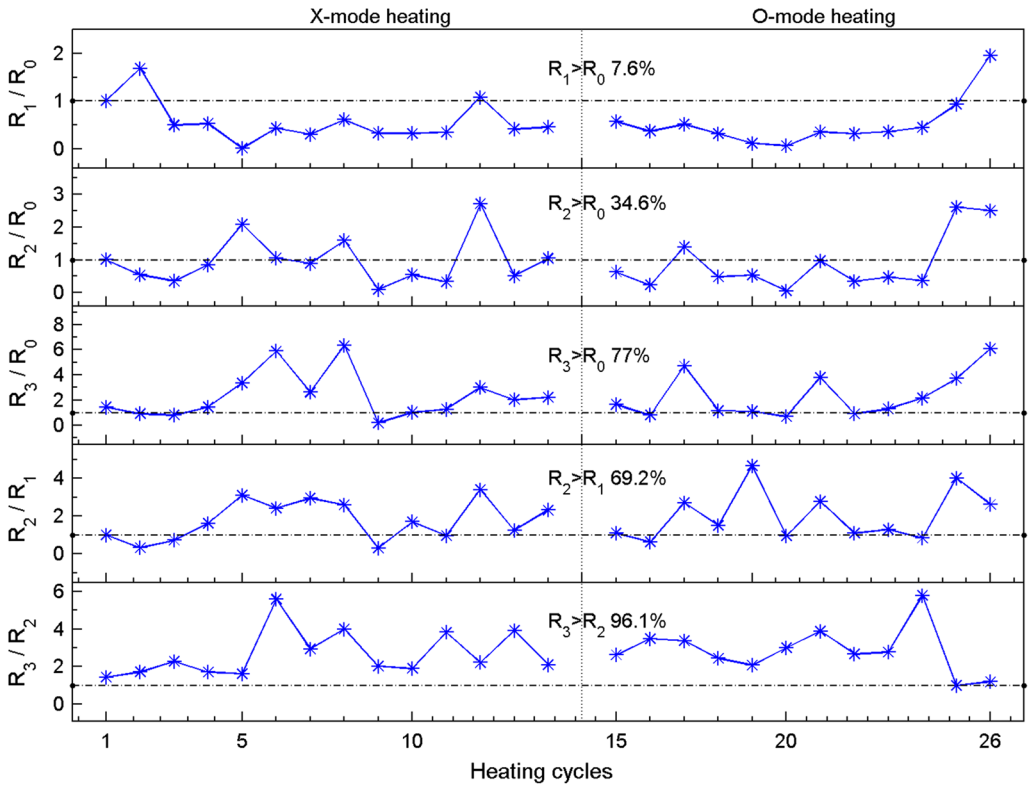

Fig. 4 As for Fig. 3 but for case 2. In this case, the HF transmitter was operated with one frequency 5.423 MHz

PMSE modulation index and enhanced electron temperature

The ratio of modulated PMSE (affected from heating) to un-modulated PMSE (unheated PMSE) is called PMSE modulation index (MI). PMSE modulation index is used to show that due to HF heating, how much the modulated PMSE varies around its un-modulated PMSE level. The PMSE modulation index (MI) represented in percentage is given as,

$$\mathrm{MI}\,(\%) = \left(\frac{\bar{R}_0 - \bar{R}_1}{\bar{R}_0}\right) \times 100 \tag{2}$$

Here, $\bar{R}_0$ is the mean of 10 data points (20 s) before the heater is switched-on, while $\bar{R}_1$ is the mean of 10 data points (20 s) after the heater has been switched-on.

To estimate the electron temperature in mesosphere, we apply the Kassa et al. (2005) heating model to investigate the relation between enhanced electron temperature and PMSE modulation index. For approximately 95% of PMSE, radars do not detect any local reduction of electrons (bite-out). Therefore, to estimate enhanced electron temperature we only use equation (15) of Kassa et al. (2005)

$$T_e \approx T_i\left(\frac{2 - \sqrt{R_1/R_0}}{\sqrt{R_1/R_0}}\right) \tag{3}$$

where T_e and T_i represent the enhanced electron temperature and background ion temperature, respectively. According to Kassa et al. (2005), visibly the temperatures of neutral and ion are unaffected by heating and equal to 150 K. Therefore, in Eq. (3) $T_i = T_{neutral} = 150$ K was used for both layers assuming that the temperatures of ion and neutral are not affected by the heater wave. R_0 and R_1 are already defined in the data analysis.

Enhanced electron temperature in lower and upper layers

Figures 7, 8, 9 and 10 show the enhanced electron temperature and PMSE modulation index for corresponding heating cycles of Figs. 3, 4, 5 and 6, respectively. Panel 1 of Figs. 7, 8, 9 and 10 shows that for most of the heating cycles, electron temperature is greater than 150 K. This indicates that due to ionospheric heating for most of the heating cycles, electron temperature increases from its background neutral or ion temperature (150 K). Furthermore, for the majority of heating cycles the enhanced

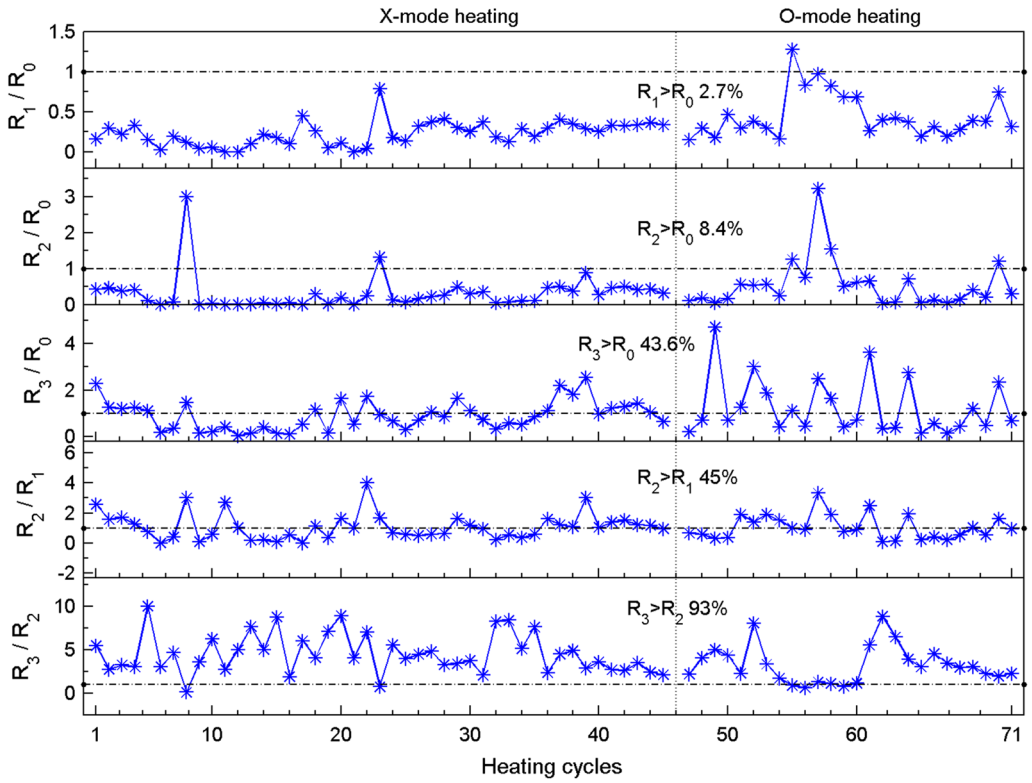

Fig. 5 As for Fig. 3 but for case 3a. In this case, the HF transmitter was operated with one frequency 5.423 MHz

electron temperature varies between 150 and 500 K. From panel 1 of Figs. 7, 8, 9 and 10, it is clear that for cases 1, 2, 3a and 3b the percentage of heating cycles having enhanced electron temperature > 500 K is 31%, 7.6%, 25.3% and 24%, respectively.

PMSE modulation index in lower and upper layers

Panel 2 of Figs. 7, 8, 9 and 10 shows that for cases 1, 2, 3a and 3b, the percentage of heating cycles having PMSE modulation index > 50% is 68.8%, 38.5%, 93% and 76%, respectively. This indicates that in all cases, there are significant numbers of cycles where PMSE was modulated due to artificial electron heating to 50% of its unheated state, i.e., $(R_0 - R_1) = (50\%)R_0$.

Discussion

In the previous section, the statistical results of modulated PMSE have been presented under the condition without high-energy particle precipitation. Now, here we will discuss the results of the different modulated PMSE characteristics and enhanced electron temperature relations with PMSE modulation index between the lower and upper PMSE layers.

Different characteristics of modulated PMSE

The OCC of VHF (224 MHz) and UHF (930 MHz) radars generally shows the 'classical drop in PMSE intensity' (Havnes et al. 2004; Næsheim et al. 2008) where usually the PMSE intensity decreases when the heater is switched-on, i.e., $R_1 < R_0$ (Chilson et al. 2000). Before the heater is switched-on, the plasma densities and dust charges are in equilibrium at temperature of 150 K. Electron temperature increases rapidly just after the heater is switched-on. This increase in electron temperature smooths the electron density profile and hence decreases the PMSE intensity. The magnitude of 'PMSE intensity decrease' is therefore mainly determined by the increase in the electron temperature (Havnes et al. 2003). Chilson et al. (2000) first observed the drop in PMSE intensity ($R_1 < R_0$) at VHF and later Næsheim et al. (2008) at UHF. Chen and Scales (2005) show that the PMSE intensity decreases when the

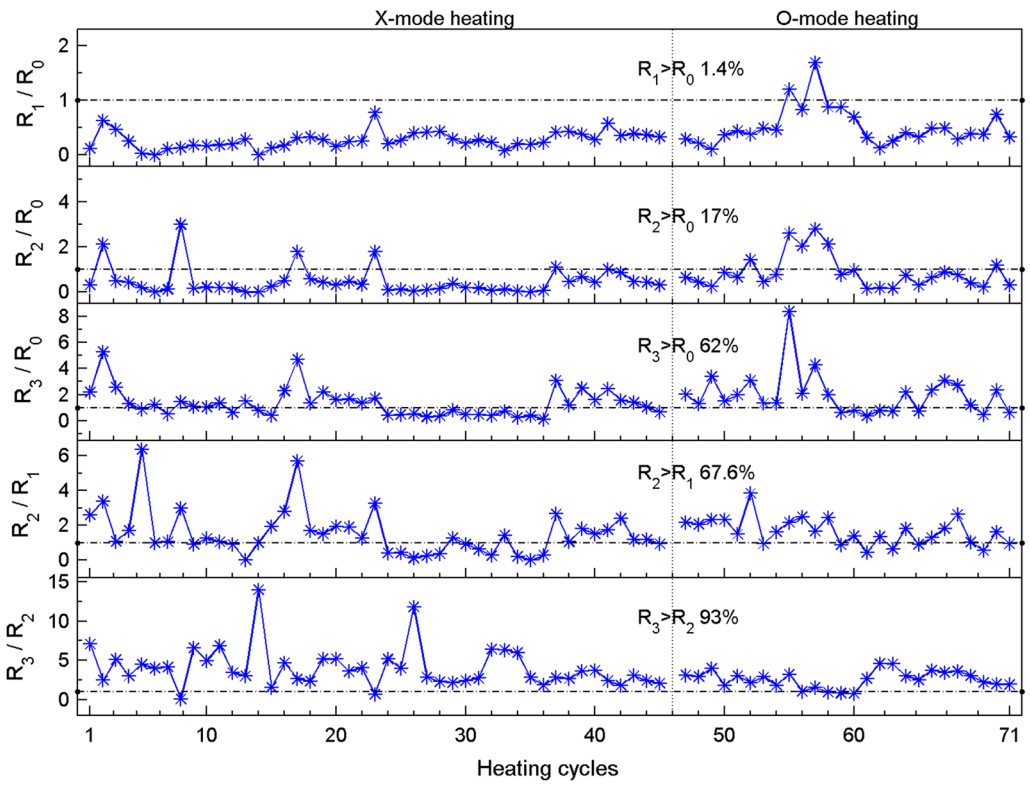

Fig. 6 As for Fig. 3 but for case 3b. In this case, the HF transmitter was operated with one frequency 5.423 MHz

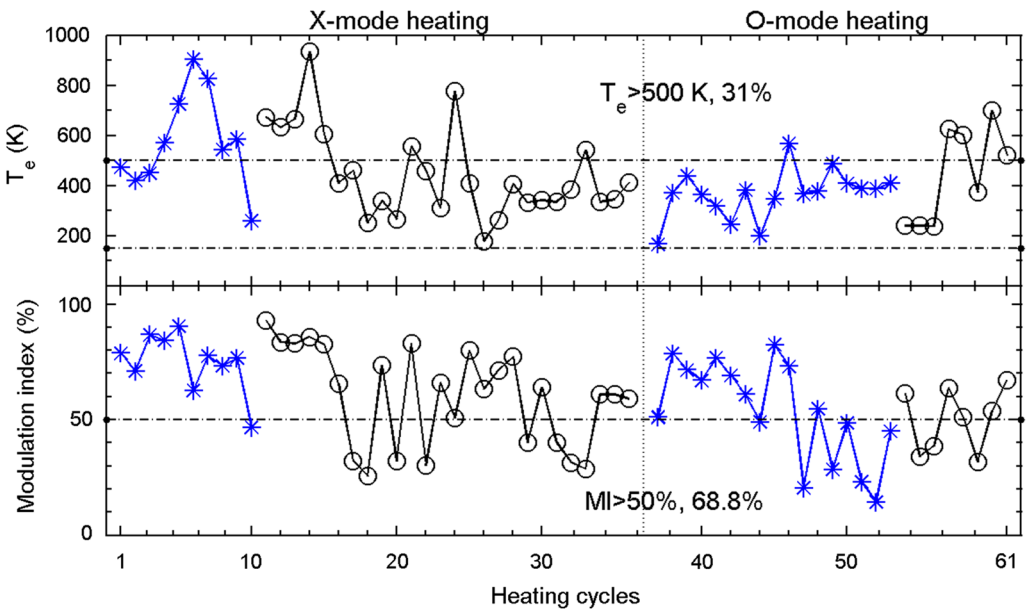

Fig. 7 Panels 1 and 2 show the enhanced electron temperature (T_e) and PMSE modulation index (MI), respectively, for corresponding heating cycles of case 1. The percentage shown in panel 1 corresponds to number of cycles where $T_e > 500$ K, while in panel 2 corresponds to number of cycles where PMSE modulation index, MI > 50%. The asterisks represent the measurements at transmitter frequency 5.423 MHz, whereas the circles represent the measurements at 7.953 MHz. The vertical dash line is used to separate the measurements of *X*- and *O*-modes polarization

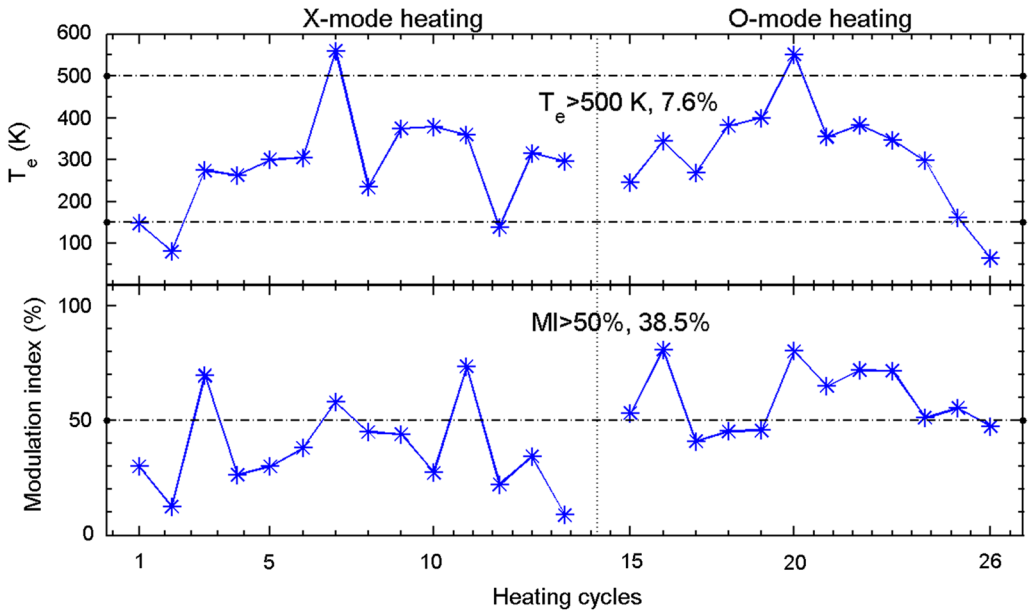

Fig. 8 As for Fig. 7 but for case 2. In this case, the HF transmitter was operated with one frequency 5.423 MHz

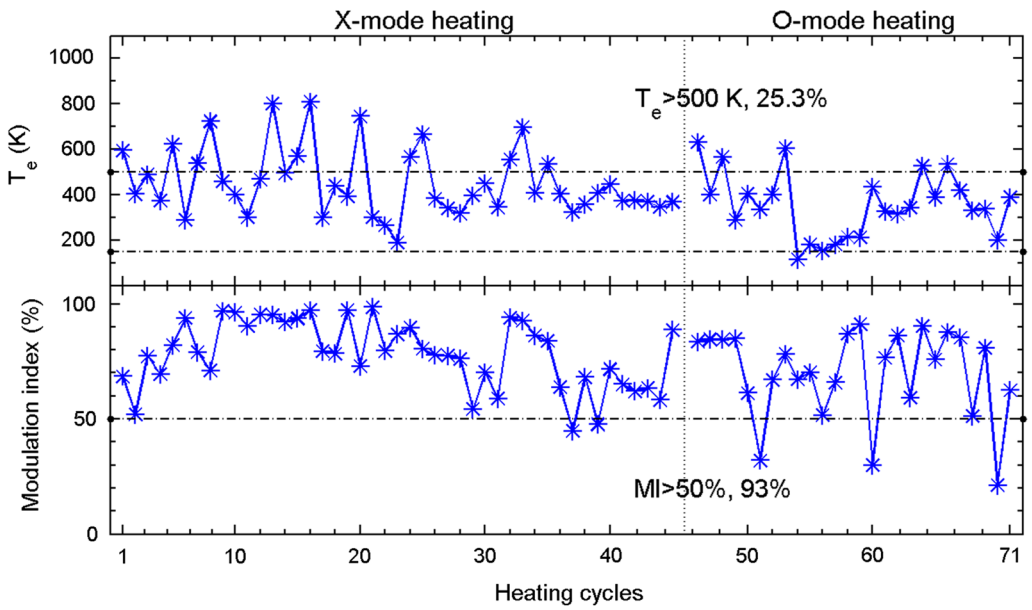

Fig. 9 As for Fig. 7 but for case 3a. In this case, the HF transmitter was operated with one frequency 5.423 MHz

gradient in electron density decreases due to small plasma adjustment time (diffusion time).

On the other hand, in panel 1 of Figs. 3, 4, 5 and 6 a few cycles also show $R_1 > R_0$. From panel 1 of Figs. 3, 4, 5 and 6, it is clear that case 2 (Fig. 4) shows comparatively greater percentage (7.6%) of $R_1 > R_0$ as compared to other cases. In these few cycles, $R_1 > R_0$ may be due to the effect of noise. This behavior ($R_1 > R_0$) is opposite to the PMSE intensity drop ($R_1 < R_0$). However, Senior et al. (2014) experimentally showed an example of this opposite behavior and Scales (2004) also predicted $R_1 > R_0$ for low-frequency (longer wavelength) radars. Havnes et al. (2015) also showed that at low frequency (56 MHz), a

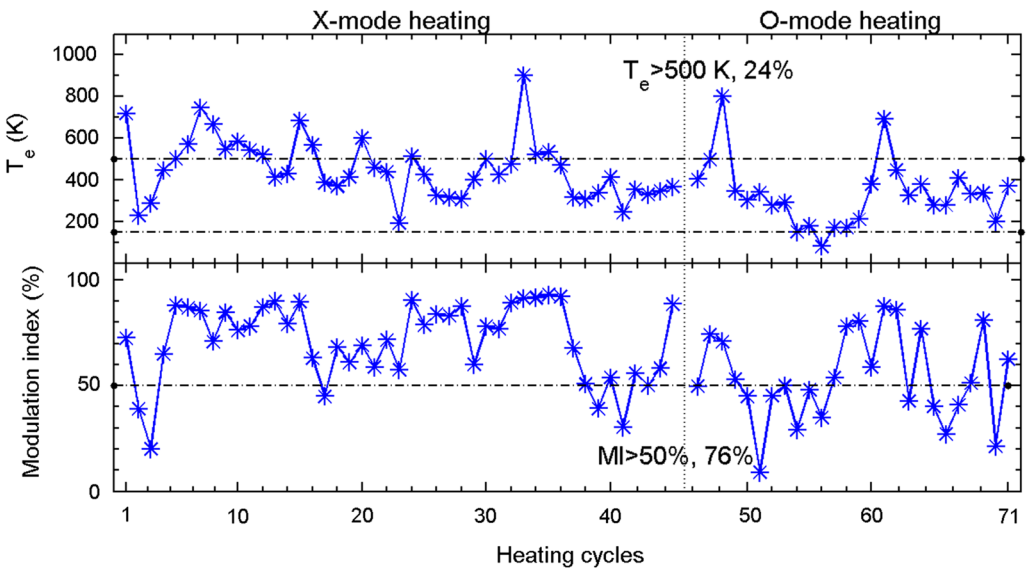

Fig. 10 As for Fig. 7 but for case 3b. In this case, the HF transmitter was operated with one frequency 5.423 MHz

significant number of cases experience $R_1 > R_0$, whereas for high frequency (224 MHz) this is rare.

During the heater-on period, the PMSE recovery due to additional charging depends mainly on the density and size of the dust particles in mesosphere. Usually, $R_2 < R_0$ but in case of PMSE recovery $R_2 > R_0$ is observed (Havnes et al. 2015). When the heater is switched-off, the recovery may smooth out or even decreases. The PMSE recovery during the heating-on period is the consequence of the larger dust size, smaller dust charging time and longer plasma adjustment time of the dust density structures (Scales 2004; Biebricher and Havnes 2012).

When the dust density is relatively low, then the dust size has a significant effect on the dust charging time. For decreasing size of dust radius, the dust charging time becomes greater than the plasma adjustment time which gives rise to the PMSE overshoot effect (Scales 2004; Chen and Scales 2005). For the ratio $R_2 > R_1$ so far, no model calculation has been made.

The rapid increase in PMSE intensity ($R_3 > R_2$) is expected from the first observations and models of overshoot effect (Havnes et al. 2003). For a significant number of cases, $R_3 < R_2$ was found by Havnes et al. (2015) for the MORRO 56 MHz radar, but for VHF observations only few cases were found with $R_3 < R_2$. The opposite behavior of $R_3 > R_2$ ($R_3 < R_2$) has been found in the model study presented by Biebricher and Havnes (2012) for frequency smaller than that of 56 MHz radar. The reason for $R_3 > R_2$ after the heater is switched-off is again the smaller dust charging time than that of the plasma adjustment time (Havnes et al. 2015).

As the edge of PMSE horizontally shifts ~2.5 km due to a drift of ~50 m/s (Havnes et al. 2015), however, we do not expect any effect on the results shown in Figs. 3, 4, 5 and 6 due to a drift of PMSE/NLC clouds because of the small observing time between the parameters (R_0, R_1, R_2, and R_3).

Several differences in the different PMSE characteristics (PMSE intensity reduction, recovery, overshoot, $R_2 > R_1$, and $R_3 > R_2$) between lower and upper PMSE layers can be attributed to the differences in neutral density and electron heating. Heating effect in the PMSE region primarily depends on electron content below the PMSE layer. In the lower layer, the charge adjustment due to higher electron temperature during the heater-on period is more rapid than that in the upper layer. On the other hand, in the upper layer due to low density of neutral gas, normally the ion and electron ambipolar diffusion is more rapid than that in the lower layer. In this way, the charge adjustment dominates in the lower layer while plasma adjustment in the upper layer of PMSE. Moreover, the heating effect in the PMSE region also has combined and complicated dependencies on electron density, dust sizes and density (Havnes 2004; Biebricher et al. 2006; Scales 2004; Biebricher and Havnes 2012; Scales and Chen 2008).

Case 1 (Figs. 3, 7) shows the effect of HF transmitter frequency on PMSE heating effect. Because only case 1 has measurements at two different transmitter frequencies (5.423 MHz and 7.953 MHz). In panels 1–5 of Fig. 3 at *O*-mode, the PMSE characteristics show no great difference at frequencies 5.423 MHz and 7.953 MHz.

However, at *X*-mode at high frequency (7.953 MHz) the PMSE characteristics are comparatively greater than that at low frequency (5.423 MHz). On the other hand, panels 1 and 2 of Fig. 7 indicate that at *X*-mode the enhanced electron temperature and PMSE modulation index show no great difference at two frequencies. However, at *O*-mode the enhanced electron temperature at high frequency (7.953 MHz) is comparatively greater than that at low frequency (5.423 MHz).

Heating effect in the presence of particle precipitation (one special case)

In heating experiments, the ionization of the middle atmosphere is very important. Large ionization due to large particle fluxes lead to high electron density, consequently most of the heater wave is absorbed and less amount of heater wave reached the upper PMSE layers (Biebricher et al. 2006). A special case in Table 1 corresponds to the heating cycles when PMSE and precipitation occur simultaneously. In Fig. 11, the precipitation for

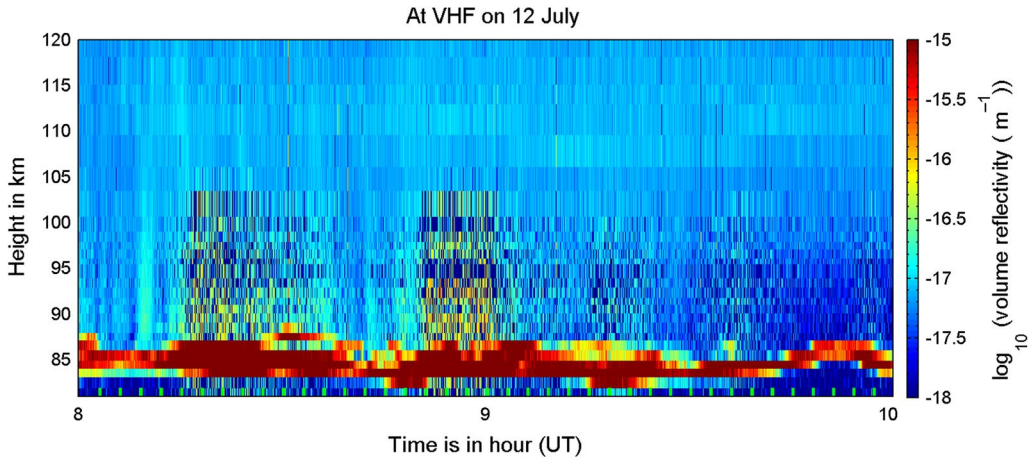

Fig. 11 An example of VHF PMSE observations in the presence of particle precipitation. The vertical green bars indicate the heater-on period

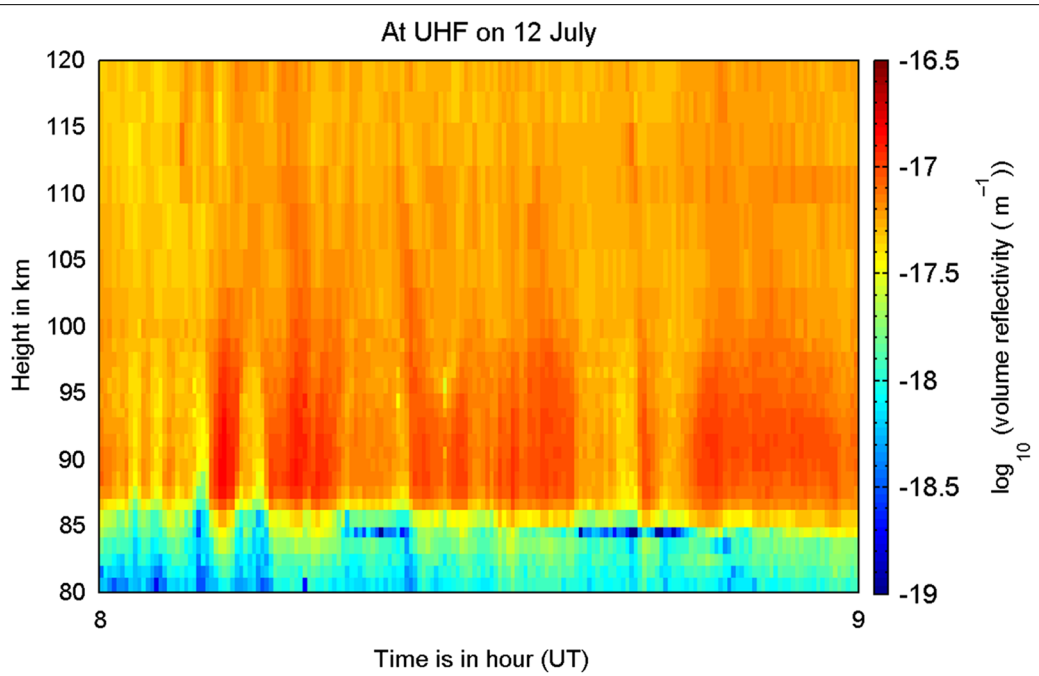

Fig. 12 UHF radar observations for the corresponding VHF radar observation (8–9 UT) of Fig. 11

cycles corresponds to time 08:15–08:30 UT and 08:50–09:00 UT seems strange and reaching in PMSE region, i.e., below 90 km. From strange, we mean that these data points satisfied the threshold of PMSE used in this paper. On the other hand, such data points extended above 90 km, while it is well known that PMSE range region is from 80 to 90 km. Therefore, to explain the VHF radar observations at these specific heating cycles, we used the observation carried out by UHF radar at the same site and time as that of VHF radar. Figure 12 shows clear precipitation with no PMSE at UHF radar. Based on UHF radar observation of Fig. 12, we conclude that the strange VHF observations at time 08:15–08:30 UT and 08:50–09:00 UT are not PMSE rather they are precipitation.

The strange VHF observation in Fig. 11 is almost certainly an artifact in the data as a result of range side lobes. The PMSE at 85 km is very strong here such that range side lobe suppression was not perfect, perhaps through the receiver being overloaded. The 64×2 μs pulse length used corresponds to 19.2 km range extent so that a strong signal at 85 km may have some residual effect on the data up to $85 + 19.2 = 104.2$ km which corresponds to the 'strange' observations.

In Fig. 13, only those heating cycles of Fig. 11 are shown where PMSE is present in the presence of particle precipitation. In both layers, only the ratio of PMSE intensity just after the heater switched-on to PMSE intensity just before the heater was switched-on (R_1/R_0) is shown. It is clear that in both layers, there are no clear variations in the ratio R_1/R_0 as compared to the variations shown in Figs. 3, 4, 5 and 6. This indicates that PMSE modulation becomes less in the presence of particle precipitation.

Relation of enhanced electron temperature with PMSE modulation index

Models have been used to evaluate the role of dusty plasma parameters during the HF heating experiments (Havnes 2004; Chen and Scales 2005). Enhanced electron temperature is one of the important physical parameters accounting for the weakening and strengthening of the mesospheric echoes. In the current article, the electron temperature in the mesosphere was estimated by using the Kassa et al. (2005) heating model. For PMSE modulation index, we have used the same length of data as in Routledge et al. (2011), i.e., mean of 10 data points before the heater-on and mean of 10 data points after the heater-on, while for the estimated electron temperature as in Kassa et al. (2005), i.e., 1 data point before and 1 data point after the heater-on. The difference is that we have used volume reflectivity instead of PMSE

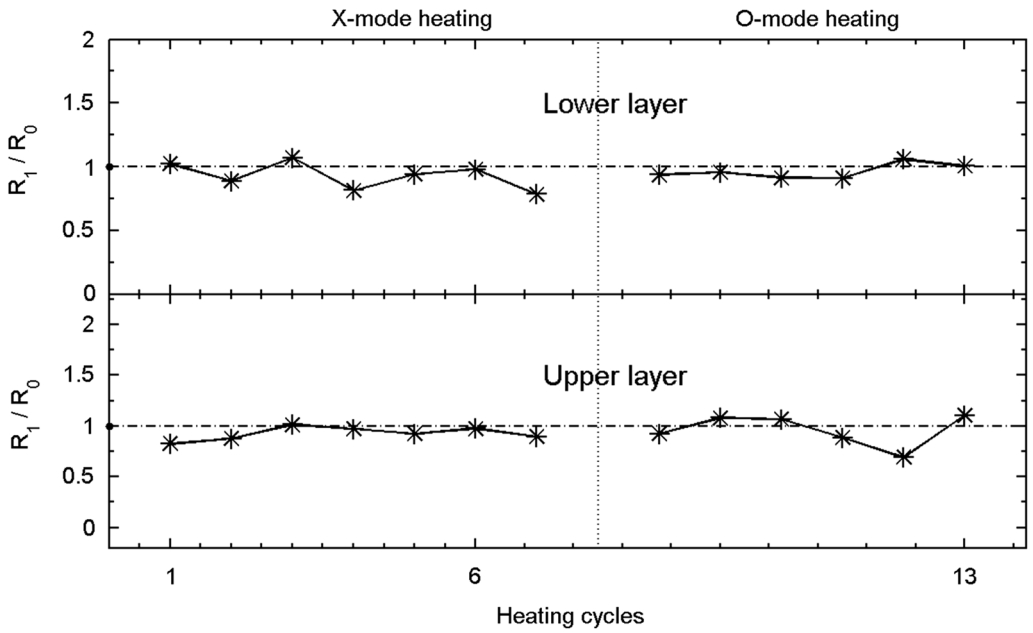

Fig. 13 Comparison of ratio R_1/R_0 in lower and upper layers for those heating cycles of Fig. 11 where precipitation and PMSE occur simultaneously. The vertical dash line is used to separate the measurements of X- and *O*-modes polarization. In this case, the HF transmitter frequency was 5.423 MHz

power. The Kassa et al. (2005) estimated electron temperature is lower than the modeled electron temperature of Routledge et al. (2011). For 50% PMSE modulation Routledge et al. (2011) and Kassa et al. (2005) require an electron temperature enhancement of 1500–2000 K and 90–100 K, respectively. In this study, all those heating cycles with PMSE modulation index $\geq 50\%$ have corresponding enhanced electron temperature > 160 K.

Our results show that in the lower PMSE layer, a greater number of heating cycles correspond to greater enhanced electron temperature and PMSE modulation than that in the upper layer. For example, comparison of cases 1 and 2 shows that in the lower layer (Fig. 7) greater number of cycles (31%) shows $T_e > 500$ K, whereas in the corresponding upper layer (Fig. 8) 7.6% of cycles show $T_e > 500$ K. Similarly, in the lower layer (Fig. 7) there are greater number of cycles (68.8%) where MI > 50%, whereas in the corresponding upper layer (Fig. 8) for 38.5% of heating cycles MI > 50%. Furthermore, in lower layer shown in Fig. 9 (case 3a) the percentage of heating cycles having $T_e > 500$ K and MI > 50% is 25.3% and 93%, respectively, whereas in the corresponding upper layer shown in Fig. 10 (case 3b) the percentage of heating cycles having $T_e > 500$ K and MI> 50% is 24% and 76%, respectively.

Conclusions

In this article, the PMSE observations carried out by EISCAT VHF radar in July 2007 in the absence of high-energy particle precipitation have been analyzed. The response of PMSE to HF heating in the lower and upper PMSE layers is studied. Different modulated PMSE characteristics (e.g., PMSE intensity reduction, recovery, overshoot, ratios during the heating-on and heating-off times) are analyzed and compared between the lower and upper layers. Based on statistical results, it is found that there is a relatively strong tendency that all these characteristics of modulated PMSE except PMSE recovery are greater in lower layer as compared to upper layer. The effect of enhanced electron temperature on PMSE is analyzed in terms of PMSE modulation index. From statistical results, it is found that in both layers usually higher enhanced electron temperature corresponds to higher PMSE modulation. Furthermore, in the lower layer enhanced electron temperature and PMSE modulation index are greater than that in the upper layer. Within PMSE layers, the variability of electron temperature enhancement may be responsible for the variations in the modulated PMSE characteristics between the lower and upper layers.

Abbreviations

PMSE: polar mesosphere summer echoes; EISCAT: European Incoherent Scatter; NLC: noctilucent clouds; VHF: very high frequency; UHF: ultra high frequency; OCC: overshoot characteristic curve; GUISDAP: Grand Unified Incoherent Scatter Design and Analysis Program.

Authors' contributions

Manuscript preparation and data analysis were done by SU and HL. AR helped in plotting figures. LM and BW gave useful suggestions in discussing the results, whereas MW helped in improving the English grammar. All authors read and approved the final manuscript.

Author details

[1] School of Electronic Science and Engineering, University of Electronic Science and Technology of China, Chengdu, China. [2] School of Physics, University of Electronic Science and Technology of China, Chengdu, China.

Acknowledgements

We appreciate the helpful assistance of Dr. Jun Wu and Professor Cesar La Hoz for providing the experimental information. The EISCAT Scientific Association is supported by China (China Research Institute of Radio wave Propagation), Finland (Suomen Akatemia of Finland), Japan (the National Institute of Polar Research of Japan and Institute for Space-Earth Environmental Research at Nagoya University), Norway (Norges Forkningsrad of Norway), Sweden (the Swedish Research Council) and the UK (the Natural Environment Research Council).

Competing interests

The authors declare that they have no competing interests.

Availability of data and materials

The radar data between July 10 and 19, 2007, are available through the EISCAT data portal at https://www.eiscat.se/schedule/schedule.cgi?year=2007&month=7&S=on&A=on&VHF=on&HEA=on.

Consent for publication

Not applicable.

Ethics approval and consent to participate

Not applicable.

Funding

This work is supported by National Natural Science Foundation of China (Grant Nos. 41104097 and 41304119) and by the National Key Laboratory of Electromagnetic Environment, China Research Institute of Radio wave Propagation (CRIRP).

Publisher's Note

Received: 27 September 2018 Accepted: 19 February 2019
Published online: 27 February 2019

References

Baron M (1986) EISCAT progress 1983–1985. J Atmos Terr Phys 48:767–772. https://doi.org/10.1016/0021-9169(86)90050-4

Belova E, Pashin AB, Lyatsky WB (1995) Passage of powerful HF radio wave through the lower ionosphere as a function of initial electron density profiles. J Atmos Terr Phys 57:265–272. https://doi.org/10.1016/0021-9169(93)E0012-X

Belova E, Chilson P, Kirkwood S, Rietveld MT (2003) The response time of PMSE to ionospheric heating. J Geophys Res. https://doi.org/10.1029/2002jd002385

Belova E, Smirnova M, Rietveld MT, Isham B, Kirkwood S, Sergienko T (2008) First observation of the overshoot effect for polar mesospheric winter echoes during radio wave electron temperature modulation. Geophys Res Lett 35:L03110. https://doi.org/10.1029/2007GL032457

Berger U, Von Zahn U (2002) Icy particles in the summer mesopause region: three-dimensional modeling of their environment and two-dimensional modeling of their transport. J Geophys Res (Space Phys) 107:1366. https://doi.org/10.1029/2001JA000316

Biebricher A, Havnes O (2012) Non-equilibrium modeling of the PMSE overshoot effect revisited: a comprehensive study. J Plasma Phys 78:303–319. https://doi.org/10.1017/S0022377812000141

Biebricher A, Havnes O, Hartquist TW, La Hoz C (2006) On the influence of plasma absorption by dust on the PMSE overshoot effect. Adv Space Res 38:2541–2550. https://doi.org/10.1016/j.asr.2005.02.061

Chen C, Scales WA (2005) Electron temperature enhancement effects on plasma irregularities associated with charged dust in the Earth's mesosphere. J Geophys Res 110:A12313. https://doi.org/10.1029/2005ja011341

Chilson PB, Belova E, Rietveld MT, Kirkwood S, Hoppe UP (2000) First artificially induced modulation of PMSE using the EISCAT heating facility. Geophys Res Lett 27:3801–3804. https://doi.org/10.1029/2000GL011897

Ecklund WL, Balsley BB (1981) Long-term observations of the arctic mesopause with the MST radar at Poker Flat, Alaska. J Geophys Res 86:7775–7780. https://doi.org/10.1029/JA086iA09p07775

Eremenko MN, Petelina SV, Zasetsky AY, Karlsson B, Rinsland CP, Llewellyn EJ, Sloan JJ (2005) Shape and composition of PMC particles derived from satellite remote sensing measurements. Geophys Res Lett 32:L16S06. https://doi.org/10.1029/2005GL023013

Friedrich M, Torkar KM, Singer W, Strelnikova I, Rapp M, Robertson S (2009) Signatures of mesospheric particles in ionospheric data. Ann Geophys 27:823–829. https://doi.org/10.5194/angeo-27-823-2009

Havnes O (2004) Polar mesospheric summer echoes (PMSE) overshoot effect due to cycling of artificial electron heating. J Geophys Res 109:A02309. https://doi.org/10.1029/2003ja010159

Havnes O, Kassa M (2009) on the sizes and observable effects of dust particles in polar mesospheric winter echoes. J Geophys Res 114:D09209. https://doi.org/10.1029/2008jd011276

Havnes O, Trøim J, Blix T, Mortensen W, Næsheim LI, Thrane E, Tønnesen T (1996) First detection of charged dust particles in the Earth's mesosphere. J Geophys Res 101:10839–10847. https://doi.org/10.1029/96ja00003

Havnes O, La Hoz C, Næsheim LI, Rietveld MT (2003) First observations of the PMSE overshoot effect and its use for investigating the conditions in the summer mesosphere. Geophys Res Lett 30:2229. https://doi.org/10.1029/2003gl018429

Havnes O, La Hoz C, Biebricher A, Kassa M, Meseret T, Næsheim LI, Zivkovic T (2004) Investigation of the mesospheric PMSE conditions by the use of the new overshoot effect. Phys Scr 107(70):78. https://doi.org/10.1238/physica.topical.107a00070

Havnes O, La Hoz C, Aylward A, Belova E, Hartquist TW, Kosch MJ, Morfill G, Jones GOL, Næsheim LI, Rietveld MT, Rubin Zuzic M, Sigernes F (2006) Observations of the overshoot effect during the 2004 EISCAT PMSE campaign. Adv Space Res 38:2344–2352. https://doi.org/10.1016/j.asr.2005.11.004

Havnes O, Pinedo H, La Hoz C, Senior A, Hartquist TW, Rietveld MT, Kosch MJ (2015) A comparison of overshoot modelling with observations of polar mesospheric summer echoes at radar frequencies of 56 and 224 MHz. Ann Geophys 33:737–747. https://doi.org/10.5194/angeo-33-737-2015

Kassa M, Havnes O, Belova E (2005) The effect of electron bite-outs on artificial electron heating and PMSE overshoot. Ann Geophys 23:3633–3643. https://doi.org/10.5194/angeo-23-3633-2005

Lehtinen MS, Huuskonen A (1996) General incoherent scatter analysis and GUISDAP. J Atmos Terr Phys 58:435–452. https://doi.org/10.1016/0021-9169(95)00047-x

Mahmoudian A, Mohebalhojeh AR, Farahani MM, Scales WA, Kosch M (2016) Remote sensing of mesospheric dust layers using active modulation of PMWE by high-power radio waves. J Geophys Res Space Phys 122:843–856. https://doi.org/10.1002/2016ja023388

Mitchell JD, Croskey CL, Goldberg RA (2001) Evidence for charged aerosols and associated meter-scale structure in identified PMSE/NLC regions. Geophys Res Lett 28:1423–1426. https://doi.org/10.1029/2000gl012685

Næsheim LI, Havnes O, LaHoz C (2008) A comparison of polar mesosphere summer echo at VHF (224 MHz) and UHF (930 MHz) and the effects of artificial electron heating. J Geophys Res 113:D08205. https://doi.org/10.1029/2007jd009245

Rapp M, Lübken F-J (2000) Electron temperature control of PMSE. Geophys Res Lett 27:3285–3288. https://doi.org/10.1029/2000gl011922

Rapp M, Lübken F-J (2003) On the nature of PMSE: electron diffusion in the vicinity of charged particles revisited. J Geophys Res 108:8437. https://doi.org/10.1029/2002jd002857

Rapp M, Thomas GE (2006) Modeling of the microphysics of mesospheric ice particles: assessment of current capabilities and basic sensitivities. J Atmos Sol Terr Phys 68:715–744. https://doi.org/10.1016/j.jastp.2005.10.015

Rietveld MT, Kohl H, Kopka H, Stubbe P (1993) Introduction to ionospheric heating at Tromsø. Part I: experimental overview. J Atmos Terr Phys 55:577–599. https://doi.org/10.1016/0021-9169(93)90007-l

Rietveld MT, Senior A, Markkanen J, Westman A (2016) New capabilities of the upgraded EISCAT high-power HF facility. Radio Sci. https://doi.org/10.1002/2016rs006093

Röttger J, La Hoz C (1990) Characteristics of polar mesosphere summer echoes (PMSE) observed with the EISCAT 224 MHz radar and possible explanations of their origin. J Atmos Sol Terr Phys 52:893–906. https://doi.org/10.1016/0021-9169(90)90023-g

Routledge G, Kosch MJ, Senior A, Kavanagh AJ, McCrea IW, Rietveld MT (2011) A statistical survey of electron temperature enhancements in heater modulated polar mesospheric summer echoes at EISCAT. J Atmos Terr Phys 73:472–482. https://doi.org/10.1016/j.jastp.2010.11.004

Scales WA (2004) Electron temperature effects on small scale plasma irregularities associated with charged dust in the earth's mesosphere. IEEE Trans Plasma Sci 32:724–730. https://doi.org/10.1109/tps.2004.826082

Scales WA, Chen C (2008) On initial enhancement of mesospheric dust associated plasma irregularities subsequent to radiowave heating. Ann Geophys 26:2265–2271. https://doi.org/10.5194/angeo-26-2265-2008

Scales WA, Mahmoudian A (2016) Charged dust phenomena in the near-Earth space environment. Rep Prog Phys 79:106802. https://doi.org/10.1088/0034-4885/79/10/106802

Senior A, Mahmoudian A, Pinedo H, La Hoz C, Rietveld MT, Scales WA, Kosch MJ (2014) First modulation of high-frequency polar mesospheric summer echoes by radio heating of the ionosphere. Geophys Res Lett 41:5347–5353. https://doi.org/10.1002/2014gl060703

Ullah S, Li H, Rauf A, Meng L, Wang B, Wang M (2018) PMSE dependence on frequency observed simultaneously with VHF and UHF radars in the presence of precipitation. Plasma Sci Technol 20:115302. https://doi.org/10.1088/2058-6272/aac8d4